

**Cu<sub>2</sub>S<sub>3</sub> complex on Cu(111) as a candidate for mass transport enhancement**Holly Walen,<sup>1</sup> Da-Jiang Liu,<sup>2</sup> Junepyo Oh,<sup>3</sup> Hyunseob Lim,<sup>3,\*</sup> J. W. Evans,<sup>2,4</sup> Christine M. Aikens,<sup>5</sup> Yousoo Kim,<sup>3</sup> and P. A. Thiel<sup>1,2,6,†</sup><sup>1</sup>*Department of Chemistry, Iowa State University, Ames, Iowa 50011, USA*<sup>2</sup>*Ames Laboratory of the USDOE, Ames, Iowa 50011, USA*<sup>3</sup>*RIKEN Surface and Interface Science Laboratory, Wako, Saitama 351-0198, Japan*<sup>4</sup>*Department of Physics & Astronomy, Iowa State University, Ames, Iowa 50011, USA*<sup>5</sup>*Department of Chemistry, Kansas State University, Manhattan, Kansas 66506, USA*<sup>6</sup>*Department of Materials Science & Engineering, Iowa State University, Ames, Iowa 50011, USA*

(Received 15 May 2014; revised manuscript received 30 December 2014; published 22 January 2015)

Sulfur-metal complexes, containing only a few atoms, can open new, highly efficient pathways for transport of metal atoms on surfaces. For example, they can accelerate changes in the shape and size of morphological features, such as two-dimensional nanoclusters, over time. In this study we perform STM under conditions that are designed to specifically isolate such complexes. We find a new, unexpected S-Cu complex on the Cu(111) surface, which we identify as Cu<sub>2</sub>S<sub>3</sub>. We propose that Cu<sub>2</sub>S<sub>3</sub> enhances mass transport in this system, which contradicts a previous proposal based on Cu<sub>3</sub>S<sub>3</sub>. We analyze bonding within these Cu-S complexes, identifying a principle for stabilization of sulfur complexes on coinage metal surfaces.

DOI: [10.1103/PhysRevB.91.045426](https://doi.org/10.1103/PhysRevB.91.045426)

PACS number(s): 68.37.Ef, 68.43.Hn

**I. INTRODUCTION**

It has been proposed that metal-adsorbate complexes can greatly accelerate rearrangements of metal nanostructures and surfaces. This issue is of importance for stability of catalysts or nanostructures, and has been the subject of prolonged speculation given that the complexity of such systems typically precludes definitive analysis [1,2]. Nonetheless, evidence continues to accumulate supporting the presence of mobile complexes on surfaces and, by implication, their role in metal transport. Recently, for instance, Parkinson *et al.* have shown that CO interacts with Pd atoms adsorbed on a Fe<sub>3</sub>O<sub>4</sub> surface, forming a highly mobile Pd-CO complex [3]. Other adsorbates that form mobile surface complexes with metals include hydrogen [4,5], oxygen [6,7], alkylsulfides [8], and—the subject of this study—sulfur [9–14]. The soft metals Cu, Ag, and Au, which are of great interest because of their catalytic and plasmonic properties, are expected to be particularly susceptible to this effect.

The challenge in identifying such complexes is their high mobility, plus their potential condensation into extended ordered structures at moderate to high coverage. Together, these considerations mean that conditions of low temperature and low coverage offer the best chance for isolating and observing such species. The present work is a search for S-Cu complexes under these conditions.

Previously, Feibelman [9] proposed that a Cu<sub>3</sub>S<sub>3</sub> complex can enhance metal transport on Cu(111), not because of high mobility (relative to metal adatoms), but rather because of high population (reflecting high stability), combined with moderate mobility (cf. Ref. [1]). The stability of the cluster was attributed to the fact that S atoms could adsorb at pseudo-fourfold-hollow (p4fh) sites created at the edges of

the metal trimer, in accord with a long-standing principle that S binds more strongly to higher-coordination sites [9,15,16]. This conjecture seemed compatible with later experimental work [10], where coarsening kinetics of Cu islands above room temperature, in the presence of adsorbed S, were interpreted in terms of Feibelman's model. However, the Cu<sub>3</sub>S<sub>3</sub> clusters were not observed directly.

In this paper we present direct evidence for an abundant small cluster that is not Cu<sub>3</sub>S<sub>3</sub>, but rather Cu<sub>2</sub>S<sub>3</sub>, on Cu(111). This cluster is immobile and stable at 5 K, where our observations are made. It forms when the Cu(111) surface is exposed to sulfur at room temperature and then quenched. Thus, it is likely to exist and participate in dynamic processes that occur at higher temperature.

**II. EXPERIMENTAL AND COMPUTATIONAL DETAILS**

All STM imaging was done at 5 K in vacuum, at a pressure lower than  $2.5 \times 10^{-11}$  Torr [17]. Assessment of the sulfur coverage  $\theta_S$  [the ratio of S atoms to Cu atoms in the (111) plane] was guided by the prior observation that a honeycomblike reconstruction first appears at  $\theta_S \sim 0.05$  [18,19]. We report S coverage on the terraces, rather than the total S coverage (which would include S at steps).

DFT calculations for surfaces used the VASP [20] code with the projector-augmented wave (PAW) method [21]. The surface was modeled by a periodic slab of  $L$  layers, separated by 1.2 nm of vacuum. Additional Cu and S atoms were added to one side of the slab. Most of the results reported used the Perdew-Burke-Ernzerhof (PBE) approximation [22] for the exchange-correlation functional. The energy cutoff for the plane-wave basis set was 280 eV. Simulated STM images were created from DFT calculations using the Tersoff-Hamman method [23,24]. Due to the existence of surface states on the Cu(111) surface,  $k$ -points convergence was slow. Averaging results for slabs of different thickness can significantly reduce the errors due to insufficient  $k$  points. Energetics reported in this paper were obtained from  $k$ -point

\*Current address: Ulsan National Institute of Science and Technology, South Korea.

†Corresponding author: [pthiel@iastate.edu](mailto:pthiel@iastate.edu)

grids that approximately correspond to  $(24 \times 24 \times 1)$  for the primitive cell, averaging results from  $L = 4$  to 7. Some key results were recalculated using DFT codes with dispersion interactions, e.g., DFT-D2 and optB88-vdW. Compared with PBE, absolute values were shifted by as much as 0.20 eV, but trends were preserved.

DFT calculations on gas phase  $\text{CuS}_2$  and  $\text{Cu}_2\text{S}_3$  molecules with varying charge states were performed with the Amsterdam density functional (ADF) code [25]. In the ADF program, the PBE functional [22] and a triple- $\zeta$  polarized (TZP) basis set with the frozen core approximation were used for geometry optimizations and Kohn-Sham orbital calculations. Relativistic effects were considered using the zeroth order regular approximation (ZORA) [26,27].

### III. IDENTIFICATION OF A $\text{Cu}_2\text{S}_3$ COMPLEX FROM STM AND DFT

The inset in Fig. 1(a) shows an image of the clean Cu(111) surface with atomic resolution. This allows us to define crystallographic directions as shown, with arrows indicating two of the six close-packed directions.

Figure 1(a) shows a representative image of S/Cu(111) terraces at lower magnification, and at  $\theta_S = 0.004$ . At this low coverage, the main features are small, uniform bright spots. Closer inspection reveals that these are actually heart-shaped clusters, as shown in Figs. 1(b)–1(d). They adopt three different orientations, rotated by  $120^\circ$ , in equal abundance. These orientations are such that the lobes of the heart align with three of the six close-packed directions of the Cu(111) surface.

We can identify the orientations of the hearts more exactly by using step edges as reference. There are two types

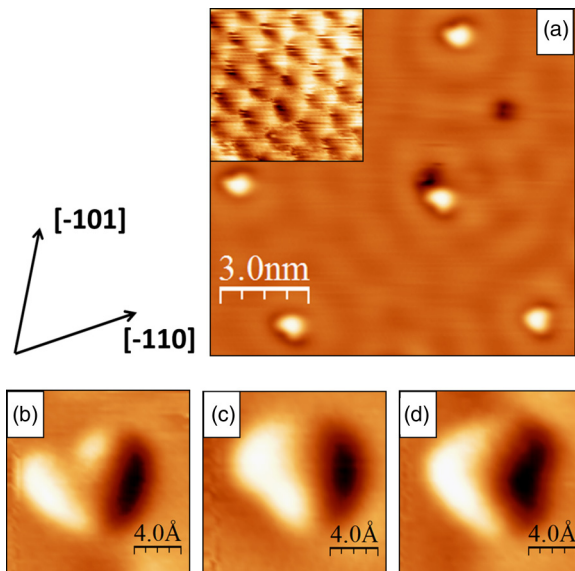


FIG. 1. (Color online) STM images of  $\text{Cu}_2\text{S}_3$  on Cu(111). (a) Several  $\text{Cu}_2\text{S}_3$  hearts on the terrace at low sulfur coverage,  $12 \times 11.5 \text{ nm}^2$ ,  $I = 1.241 \text{ nA}$ ,  $V_S = -2.000 \text{ V}$ , inset: atomic resolution of clean Cu(111);  $1.2 \times 1.2 \text{ nm}^2$ ,  $I = 1.717 \text{ nA}$ ,  $V_S = -0.004 \text{ V}$ . (b)–(d) Derivative images of the three orientations of the hearts,  $1.5 \times 1.5 \text{ nm}^2$ , (b)  $I = 1.167 \text{ nA}$ ,  $V_S = -0.004 \text{ V}$ , (c)  $I = 1.292 \text{ nA}$ ,  $V_S = -0.020 \text{ V}$ , and (d)  $I = 1.055 \text{ nA}$ ,  $V_S = -0.050 \text{ V}$ .

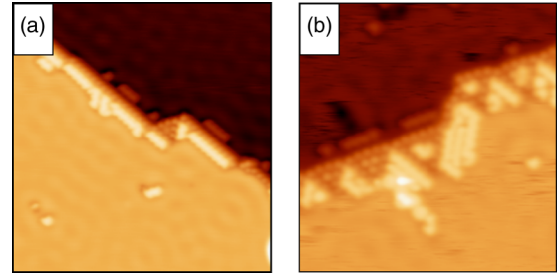


FIG. 2. (Color online) Topographic STM images of the two step edge types with S adsorption. (a) A-type (100-microfacet) edge;  $20 \times 20 \text{ nm}^2$ ,  $I = 1.241 \text{ nA}$ ,  $V_S = -0.002 \text{ V}$ . (b) B-type (111-microfacet) edge;  $15 \times 15 \text{ nm}^2$ ,  $I = 0.648 \text{ nA}$ ,  $V_S = -0.050 \text{ V}$ .

of close-packed step edges in an fcc system. These are commonly denoted A and B, where A is a (100) microfacet exposing p4fh sites, and B is a (111) microfacet exposing p3fh sites. In experiment, both types of steps exist on the clean surface and they are not easily distinguishable. Sulfur adsorbs preferentially at steps and fully decorates the steps, even at lowest  $\theta_S$ , in our experiments. After adsorption of sulfur, one type of step is long and straight, as exemplified in Fig. 2(a), while the other has a faceted sawtooth structure, as shown in Fig. 2(b) [18,19]. Notably, the inner edges of the sawtooth have the same orientation as the more extended, straight steps. We identify the straight steps as A steps because these naturally present p4fh adsorption sites where S is more stable. Using this as reference, our STM images show that the heart-shaped clusters are oriented *exclusively* with their lobes toward downgoing B steps.

We attribute the hearts to  $\text{Cu}_2\text{S}_3$  clusters of the type shown in Fig. 3(a). There is one S atom on the upper side of the Cu dimer in the figure, in a p4fh site formed by the Cu dimer plus two Cu atoms in the terrace. There are two S atoms on the lower side of the Cu dimer, each near a 3fh site on the terrace

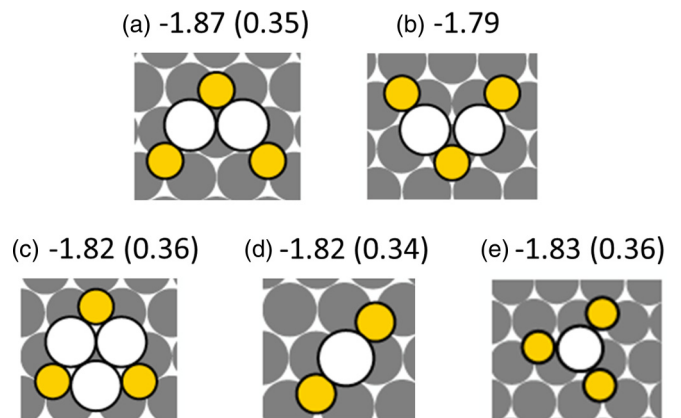


FIG. 3. (Color online) Cu-S clusters on Cu(111) with lowest chemical potentials. Values of  $\mu_S$  are given in eV. Diffusion barriers  $E_d$  are given in parentheses, also in eV. White circles represent Cu adatoms, small yellow (on-line) are S adatoms, and gray are Cu atoms in the Cu(111) surface. (a) and (b) Different configurations of  $\text{Cu}_2\text{S}_3$ , (c) is  $\text{Cu}_3\text{S}_3$ , (d) is  $\text{CuS}_2$ , and (e) is  $\text{CuS}_3$ .

and adjoining one of the Cu atoms in the dimer. These would shape the lobes of the heart.

We have used density functional theory (DFT) to check whether this assignment is reasonable in terms of stability, shape, orientation, and density. A variety of possible adsorbed clusters, with optimized configurations, are represented in Fig. 3. The chemical potential of S in Cu<sub>m</sub>S<sub>n</sub>(μ<sub>S</sub>) and the complex diffusion barrier (E<sub>d</sub>) appear at the top of each panel. μ<sub>S</sub> is defined as

$$\mu_S(\text{Cu}_m\text{S}_n) = [E(\text{Cu}_m\text{S}_n + \text{slab}) - E(\text{slab}) - m\mu_{\text{Cu}}]/n - E(\text{S}_{2,g})/2, \quad (1)$$

where  $E$  is energy,  $\mu_{\text{Cu}}$  is the cohesive energy of a bulk Cu atom, and  $m$  and  $n$  are the number of Cu and S atoms in the complex, respectively. By this definition,  $\mu_S$  measures the decrease in energy per S when a limited supply of atomic S on terraces is incorporated into clusters (given an unlimited supply of metal atoms available from steps). This equation also defines the energy of gaseous S<sub>2</sub> as the reference point for  $\mu_S$ .

A related quantity, the formation energy  $E_{\text{form}}$  is defined by

$$E_{\text{form}}(\text{Cu}_m\text{S}_n) = n[\mu_S(\text{Cu}_m\text{S}_n) - \mu_S(\text{S})]. \quad (2)$$

$E_{\text{form}}$  gives the energy cost to create a Cu<sub>m</sub>S<sub>n</sub> complex by extracting  $m$  Cu atoms from the step edge and combining them with  $n$  S atoms already on the terrace. However, Eq. (2) includes  $\mu_S(\text{S})$ , which varies with  $\theta_S$ . Since we are dealing with low  $\theta_S$ , we choose the value of  $\mu_S(\text{S})$  that is calculated from DFT for a “large” 4 × 4 supercell, corresponding to  $\theta_S = 0.0625$  ML, which is  $\mu_S(\text{S}) = -1.91$  eV. The sulfur atoms are in fcc sites. This results in the values of  $E_{\text{form}}$  shown in Table I for the optimized configurations of several Cu-S complexes. To facilitate comparisons, the values of  $\mu_S$  and  $E_d$  are also shown.

The Cu<sub>2</sub>S<sub>3</sub> complex in Fig. 3(a) has lower  $\mu_S$  than any others we have found. The three next-best complexes are shown in Figs. 3(c)–3(e). However, the ordering of  $\mu_S$  for various complexes can be sensitive to the dimension and orientation of the supercell, meaning that lateral interactions between complexes can affect the relative energies significantly. These are best taken into account by comparing  $\mu_S$ , not at fixed supercell size as in Fig. 3, but rather at fixed  $\theta_S$ , as in Fig. 4. At all  $\theta_S$ ,  $\mu_S$  of Cu<sub>2</sub>S<sub>3</sub> is lower than  $\mu_S$  of Cu<sub>3</sub>S<sub>3</sub>, and at most coverages, it is below  $\mu_S$  of atomic adsorbed S.

Second, we have simulated the shape of the complexes using the Tersoff-Hamman method [23,24]. Results are shown in Fig. 5, where Figs. 5(a) and 5(b) correspond to the

TABLE I. Energetic values calculated from VASP for optimized configurations of several Cu-S complexes, and an isolated Cu atom, on Cu(111).

Complex	$\mu_S$ , eV	$E_d$ , eV	$E_{\text{form}}$ , eV
Cu atom at an fcc terrace site	n/a	0.05	+0.78
CuS	-1.24	0.33	+0.67
CuS <sub>2</sub>	-1.82	0.34	+0.15
CuS <sub>3</sub>	-1.83	0.36	+0.24
Cu <sub>2</sub> S <sub>3</sub>	-1.87	0.35	+0.11
Cu <sub>3</sub> S <sub>3</sub>	-1.82	0.36	+0.24

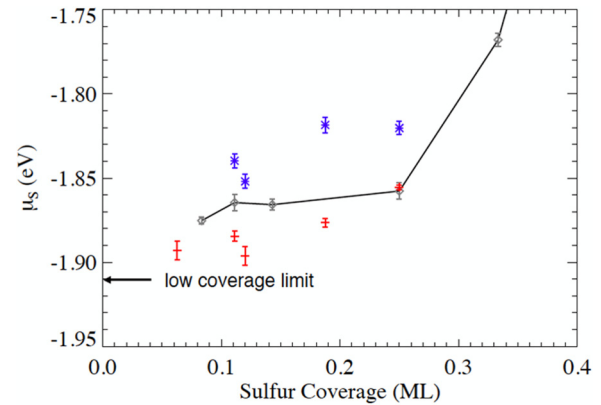


FIG. 4. (Color online) Comparison between  $\mu_S$  for Cu<sub>2</sub>S<sub>3</sub> (red pluses) and Cu<sub>3</sub>S<sub>3</sub> (blue asterisks) with that of S adatom (gray line and gray circles) on fcc sites of the Cu(111) surface. Results for various supercell sizes and azimuthal orientations are plotted as a function of S coverage.

configurations shown in Figs. 3(a) and 3(c), respectively. The heart shape is evident for Cu<sub>2</sub>S<sub>3</sub>, whereas Cu<sub>3</sub>S<sub>3</sub> is threefold symmetric and incompatible with the data. Furthermore, the area of the simulated Cu<sub>2</sub>S<sub>3</sub> complex is 0.40–0.42 nm<sup>2</sup>, in good agreement with the experimental result (0.39 ± 0.04 nm<sup>2</sup>).

Third, to understand orientation, we compare the two Cu<sub>2</sub>S<sub>3</sub> complexes shown in Figs. 3(a) and 3(b). The one in Fig. 3(a) can have three energetically equivalent orientations. In each orientation, there is one S atom in a p4fh site and two S atoms in asymmetrical sites. Considering the pair of Cu atoms as a one-dimensional step edge, one S atom lies along an A step, and the others (comprising the lobes) are along a B step. This is exactly the experimental observation. On the other hand, the complex in Fig. 3(b) has one S atom along a B step, and the lobes along an A step, inconsistent with the data. The stability of complex (a) can be rationalized by the presence of one S atom in a p4fh site, whereas (b) has none.

Finally, we consider whether the observed density of complexes is consistent with the above energetics. A simple Boltzmann factor analysis given the positive formation energy implies that the density predicted under preparation conditions at 300 K should exceed the static density observed at the lower observation temperature (5 K). (The density observed at 5 K should reflect the equilibrium density for the temperature at which the complexes are frozen in place

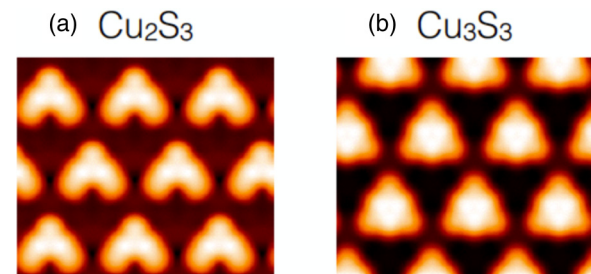


FIG. 5. (Color online) Shapes of two complexes, Cu<sub>2</sub>S<sub>3</sub> and Cu<sub>3</sub>S<sub>3</sub> on Cu(111), simulated from DFT.

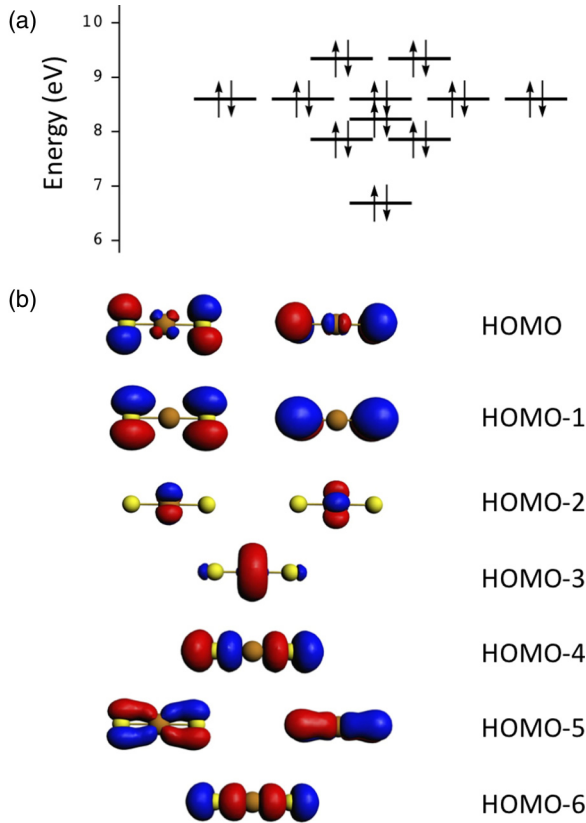


FIG. 6. (Color online) (a) PBE/TZP orbital energy diagram and (b) Kohn-Sham orbitals for  $\text{CuS}_2^{3-}$ .

during cooling. This freeze-in temperature lies between 300 and 5 K, but is otherwise unknown.) The formation energy for  $\text{Cu}_2\text{S}_3$  is +0.11 eV, so the equilibrium population predicted at 300 K is  $0.25/\text{nm}^2$ . This is well above the observed value of  $0.02/\text{nm}^2$ . Hence the two values are consistent.

#### IV. FACTORS THAT STABILIZE Cu-S COMPLEXES

The existence of  $\text{Cu}_2\text{S}_3$  complexes is surprising, given that analogous clusters have not been observed (to our knowledge) in other surface systems. To understand why they exist, we

first recall the well-known principle governing S adsorption on metal surfaces, which is that S bonds preferentially at 4fh sites, and in some cases metal surfaces rearrange to provide such sites [16]. The stability of the (hypothetical)  $\text{Cu}_3\text{S}_3$  complex, for instance, was attributed to S atoms occupying three p4fh sites at the edges of the metal trimer [9] [Fig. 3(c)]. However, in the  $\text{Cu}_2\text{S}_3$  cluster, two of the p4fh sites are sacrificed by virtue of the missing Cu atom. Thus, a factor must exist that competes with, or complements, the influence of the 4fh site. We suggest that this is the formation of linear S-Cu-S units. The  $\text{Cu}_2\text{S}_3$  complex consists of two such linear units, sharing a S atom at the apex. Adding a Cu atom to form  $\text{Cu}_3\text{S}_3$  breaks the linearity of the individual S-Cu-S units, as can be discerned in Fig. 3(c).

Insight into this configuration can be developed by starting with the isolated gas-phase  $\text{CuS}_2$  molecule, where we define the  $z$  axis as the internuclear axis. In a linear ligand field, the Cu  $d$  orbitals split into two sets of doubly degenerate orbitals,  $(d_{x^2-y^2}, d_{xy})$  and  $(d_{xz}, d_{yz})$ , and a nondegenerate  $d_{z^2}$  orbital. Of these, the  $d_{z^2}$  orbital is positioned for the best overlap with ligand  $s$  or  $p$  orbitals, followed by the  $(d_{xz}, d_{yz})$  set and finally the essentially nonbonding  $(d_{x^2-y^2}, d_{xy})$  set.

The calculated Kohn-Sham molecular orbitals for  $\text{CuS}_2^-$  at the PBE/TZP level of theory agree with this picture. Kohn-Sham orbitals for  $\text{CuS}_2$  are shown in Fig. 6 (the  $-3$  charge state is shown here; different charge states vary in their occupation of the HOMO). The lowest energy orbital shown here (HOMO-6) is a bonding interaction between the Cu  $d_{z^2}$  orbital and the S  $2p_z$  orbitals.  $\pi$ -like orbitals between Cu  $d_{xz}$  and  $d_{yz}$  and the corresponding S  $2p_x$  and  $2p_y$  atomic orbitals also aid in the strong bonding interaction. In  $\text{Cu}_2\text{S}_3$  the Kohn-Sham orbitals are spread throughout the entire  $\text{Cu}_2\text{S}_3$  unit, but the origin of the bonding still arises from Cu  $d - S 2p$  interactions as in the  $\text{CuS}_2$  picture.

Hence, linearity of the S-Cu-S unit is favored in isolated molecules because it maximizes overlap between Cu  $d_{z^2}$  and S  $2p_z$  orbitals. Analysis of VASP-based isodensity plots of adsorbed Cu-S complexes reveals that this trend is preserved on the surface. The isodensity plots for  $\text{CuS}_2$  generated from VASP (Fig. 7) show similar results for the lowest energy orbitals. Isodensity plots for states 3 and 4 for one Cu layer ( $L = 1$ ) display the bonding and antibonding configurations of the  $\text{CuS}_2$  HOMO-6 orbital with the Cu

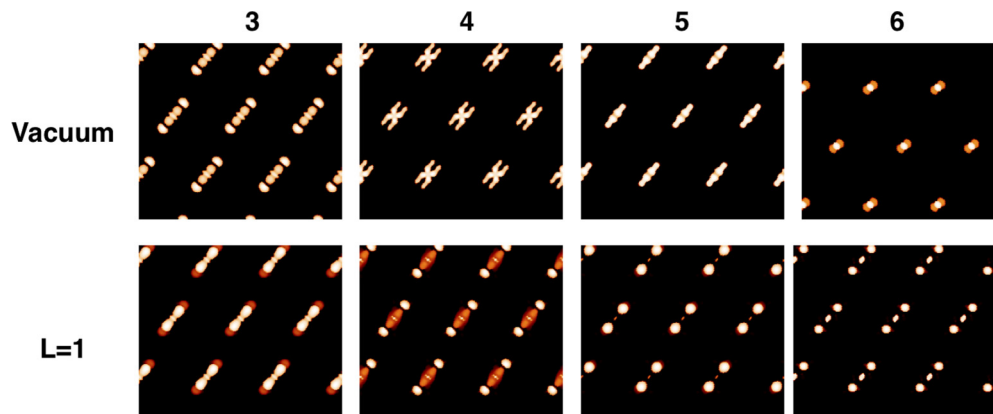


FIG. 7. (Color online) VASP isodensity plots for low energy bonding states of  $\text{CuS}_2$  in vacuum and on one layer ( $L = 1$ ) of Cu substrate.

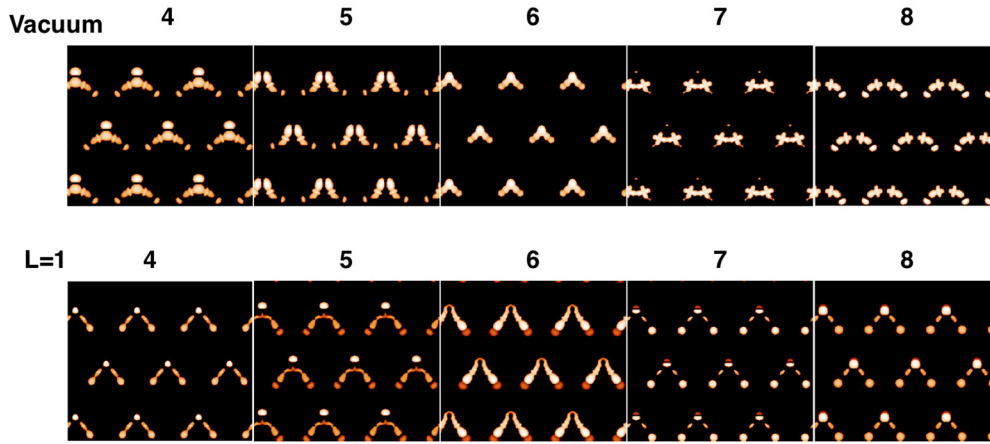


FIG. 8. (Color online) VASP isodensity plots for low energy bonding states of Cu<sub>2</sub>S<sub>3</sub> in vacuum and on one layer ( $L = 1$ ) of Cu substrate.

substrate. A small energy splitting indicates that there is a weak interaction between this orbital and the Cu substrate. Isodensity plots for states 5 and 6 for  $L = 1$  show bonding interactions between S  $2p$  orbitals that are perpendicular to the plane of the Cu surface and the underlying Cu layer. This indicates that the stability of the CuS<sub>2</sub> units on the surface can be understood both in terms of the S-Cu-S interactions and the S-surface interactions. Isodensity plots for Cu<sub>2</sub>S<sub>3</sub> in vacuum and on one layer of Cu substrate are shown in Fig. 8. The  $2p$  orbitals of the S atom at the apex have a different symmetry than those of the rest of the S atoms in the complex. One S  $2p$  orbital is perpendicular to the Cu atoms within the complex, the lower lobe of which interacts with the two Cu  $d_{z^2} S p_z$  orbitals, shown as vacuum state 4 in Fig. 8. Another S  $2p$  orbital is parallel to the Cu atoms in the complex, and each lobe interacts separately with the Cu  $d_{z^2} S p_z$  orbitals, shown as vacuum state 5 in Fig. 8. These bonding interactions are also present for the complex on one Cu layer. States 4 and 5 in vacuum become states 5 and 6 with  $L = 1$ . In addition, low energy states exhibit isodensity plots with significant S  $2p$  character perpendicular to the surface (e.g., the  $L = 1$  state 4 in Fig. 8). Again, the stability of Cu<sub>2</sub>S<sub>3</sub> is represented by the linear S-Cu-S interactions and the S-surface interactions.

In fact, linear S-M-S units are known in some related systems. Thiolates adsorbed on Au(111) [8,28], and thiolates at the periphery of Au nanoclusters, form species that include linear S-M-S units [28,29]. Linear S-M-S complexes (without alkyl ligands) have also been postulated—but not observed directly—on the basis of DFT and experimental data for S/Ag(100) [14], and on the basis of DFT alone for S/Ag(111) [2]. These results suggest that the linear S-M-S unit has generic stability across coinage metals. This is thus a complementary principle for understanding and predicting stability of S-induced structures on metal surfaces.

## V. ROLE OF Cu<sub>2</sub>S<sub>3</sub> COMPLEXES IN Cu MASS TRANSPORT

The remaining issue to be addressed is the role of the Cu<sub>2</sub>S<sub>3</sub> complex in mass transport, relative to other complexes. For a realistic analysis, one must consider a coupled set of nonlinear steady-state reaction-diffusion equations (RDEs) describing the formation, dissociation, and diffusion of various possible complexes [10,12]. Given that CuS<sub>3</sub> is reasonably stable and

is a natural precursor to Cu<sub>2</sub>S<sub>3</sub>, we focus on the reaction  $\text{Cu} + \text{CuS}_3 \leftrightarrow \text{Cu}_2\text{S}_3$ , and let  $F$  ( $R$ ) denote the rate for the forward (reverse) process, so that, e.g.,  $F = (D_{\text{Cu}} + D_{\text{CuS}_3})\theta_{\text{Cu}}\theta_{\text{CuS}_3}$ , one obtains [12]

$$\begin{aligned} \partial\theta_{\text{Cu}}/\partial t &= D_{\text{Cu}}\nabla^2\theta_{\text{Cu}} - F(\text{Cu} + \text{CuS}_3) \\ &\quad + R(\text{Cu} + \text{CuS}_3) - \dots \approx 0, \\ \partial\theta_{\text{Cu}_2\text{S}_3}/\partial t &= D_{\text{Cu}_2\text{S}_3}\nabla^2\theta_{\text{Cu}_2\text{S}_3} + F(\text{Cu} + \text{CuS}_3) \\ &\quad - R(\text{Cu} + \text{CuS}_3) + \dots \approx 0, \dots \end{aligned} \quad (3)$$

where  $D$  is the diffusion coefficient, and implicit terms account for contributions from other reactions. A typical feature of surface mass transport is that it is driven by weak spatial variations (and accompanying gradients) in coverages relative to their uniform quasiequilibrium values. Thus, it is natural to write  $\theta_{\text{Cu}} = \theta_{\text{Cu}}^{\text{eq}} + \delta\theta_{\text{Cu}}$ , etc., and to linearize the above RDE, which results in equations of the form [12]

$$\begin{aligned} \nabla^2\delta\theta_{\text{Cu}} - \delta\theta_{\text{Cu}}/L_{\text{Cu}}(\text{CuS}_3)^2 + \dots &\approx 0 \\ \text{with } L_{\text{Cu}}(\text{CuS}_3) &= [D_{\text{Cu}}/k_{\text{Cu}}(\text{CuS}_3)]^{1/2} \\ \text{and } k_{\text{Cu}}(\text{CuS}_3) &= (D_{\text{Cu}} + D_{\text{CuS}_3})\theta_{\text{CuS}_3}^{\text{eq}}, \text{ etc.} \end{aligned} \quad (4)$$

DFT indicates that  $D_{\text{Cu}} \gg D_{\text{CuS}_3}$ , so one has

$$L_{\text{Cu}}(\text{CuS}_3) \approx [\theta_{\text{CuS}_3}^{\text{eq}}]^{-1/2} \quad (5)$$

with  $\theta_{\text{CuS}_3}^{\text{eq}} = \exp[-\beta E_{\text{form}}(\text{CuS}_3)](\theta_{\text{S}})^3$ , where  $L_{\text{Cu}}(\text{CuS}_3)$  is the reaction length describing how far Cu diffuses before reacting with CuS<sub>3</sub> to form Cu<sub>2</sub>S<sub>3</sub> at rate  $k_{\text{Cu}}$ .

Further analysis of behavior requires specification of the conditions under which complexes form. In one scenario, complexes are formed by Cu and S *on terraces*; only Cu adatoms detach/attach at step edges, without any barrier except the terrace diffusion barrier [10]. However, in order for complexes to contribute to mass transport, there must be sufficient probability that they form on the terraces within a length scale much shorter than the average mass transport distance  $L_{\text{av}}$ . In other words, any gradient in  $\theta_{\text{Cu}}$  must couple sufficiently to that of  $\theta_{\text{Cu}_2\text{S}_3}$ . From (4), this requires that the reaction length be significantly smaller than the average mass transport distance. Then there is an enhanced flux  $J_{\text{Cu}_2\text{S}_3} \sim D_{\text{Cu}}\theta_{\text{Cu}}^{\text{eq}}/L_{\text{Cu}}$  in the presence of S, vs  $J_{\text{Cu}} \sim D_{\text{Cu}}\theta_{\text{Cu}}^{\text{eq}}/L_{\text{av}}$  without S.

To give a concrete example, consider the case of sulfur-enhanced Cu island coarsening on Cu(111), where the transport distance becomes the island separation. Under the experimental conditions used by Ling *et al.* [10],  $L_{av} \approx 1 \mu\text{m}$ . This is a factor of 10 smaller than the reaction length  $L_{Cu}(\text{CuS}_3) \approx 10 \mu\text{m}$ , calculated from Eq. (5) using  $T = 490 \text{ K}$  [10],  $\theta_S \approx 6 \times 10^{-3} \text{ ML}$  [10], and  $E_{\text{form}}(\text{CuS}_3) = +0.24 \text{ eV}$  as given in Table I. Hence, a diffusing Cu atom is far more likely to be captured by a Cu island than it is to form a complex on the terrace. We also note that if  $L_{Cu}(\text{CuS}_3)$  was below  $L_{av}$ , then the enhanced flux  $J_{\text{Cu}_2\text{S}_3}$  would scale like  $(\theta_S)^{3/2}$  contrasting experiment [10].

Thus, this picture does not allow enhanced mass transport by  $\text{Cu}_2\text{S}_3$  formed on terraces. If the carrier is  $\text{Cu}_3\text{S}_3$  formed from the reaction  $\text{Cu} + \text{Cu}_2\text{S}_3 \leftrightarrow \text{Cu}_3\text{S}_3$  on terraces, a similar analysis shows that  $L_{Cu}(\text{Cu}_2\text{S}_3)$  far exceeds  $L_{\text{isl}}$ , so mass transport cannot be dominated by  $\text{Cu}_3\text{S}_3$  formed on terraces, either. Analogous to the above, even if  $L_{Cu}(\text{Cu}_2\text{S}_3)$  was below  $L_{\text{isl}}$ , the corresponding enhanced flux  $J_{\text{Cu}_2\text{S}_3}$  would scale like  $(\theta_S)^{3/2}$ , contrasting experiment [10].

We propose an alternative picture where complexes attach and detach directly from step edges and their coverage at step edges is determined by their local chemical potential, which depends on step edge curvature. Then they directly contribute to mass transport, and the associated mass current of a complex C can be estimated from  $J_C \sim D_C \theta_C^{\text{eq}} \sim \exp[-E_{\text{OR}}(C)/(k_B T)]$  where  $E_{\text{OR}}(C) = E_d(C) + E_{\text{form}}(C)$ . Thus, the species with the lowest  $E_{\text{OR}}$  should dominate mass transport. Values of  $E_d$  and  $E_{\text{form}}$  for the clusters can be taken from Fig. 3 and Eq. (2), and for Cu atoms from Ref. [30]. This leads to values of  $E_{\text{OR}} = 0.91, 0.49, 0.46,$  and  $0.60 \text{ eV}$  for Cu,  $\text{CuS}_2$ ,  $\text{Cu}_2\text{S}_3$ , and  $\text{Cu}_3\text{S}_3$ , respectively. Therefore,  $\text{Cu}_2\text{S}_3$  should be the dominant mass carrier, with  $\text{CuS}_2$  also playing a possible role. The above expression for the mass current due to  $\text{Cu}_2\text{S}_3$  is consistent with the observed third-order kinetics in the S coverage using that  $\theta_{\text{Cu}_2\text{S}_3}^{\text{eq}} = \exp[-\beta E_{\text{form}}(\text{Cu}_2\text{S}_3)](\theta_S)^3$ . We also note the likelihood that there is an extra attachment barrier inhibiting the decomposition of  $\text{Cu}_2\text{S}_3$  at S-decorated step edges and incorporation of the Cu. This would explain the attachment-limited kinetics observed at intermediate  $\theta_S$  in the experimental data [10].

## VI. CONCLUSIONS

In summary, the predominant S-induced features on the Cu(111) terraces, at very low S coverages, are heart-shaped protrusions. DFT supports their assignment as  $\text{Cu}_2\text{S}_3$  clusters. These clusters are always oriented such that the lobes of the heart point toward downgoing B steps, because this allows one S atom in the cluster to bond at a p4fh site. This is different than any type of metal-sulfur surface complex observed previously, to our knowledge. It may reflect the stability of linear S-metal-S geometries. Kinetic analysis shows that  $\text{Cu}_2\text{S}_3$  is more important than  $\text{Cu}_3\text{S}_3$  in mass transport.

## ACKNOWLEDGMENTS

The experimental component of this work was supported by several sources. From the U.S., it was NSF Grant CHE-1111500. From Japan, support was provided by a Grant-in-Aid for Scientific Research on Priority Areas ‘‘Electron Transport Through a Linked Molecule in Nano-scale’’; and a Grant-in-Aid for Scientific Research(S) ‘‘Single Molecule Spectroscopy using Probe Microscope’’ from the Ministry of Education, Culture, Sports, Science, and Technology (MEXT). The theoretical analysis of kinetics was also supported by NSF Grant CHE-1111500. The DFT analysis of the energetics of chemisorbed complexes and of simulated STM images was supported by the Division of Chemical Sciences, Basic Energy Sciences, US Department of Energy (USDOE), and it utilized resources of the National Energy Research Scientific Computing Center, which is supported by the Office of Science of the US Department of Energy (Contract No. DE-AC02-05CH11231). The theoretical molecular orbital analysis for gas phase species was supported by the National Science Foundation under Grant No. CHE-1213771. C.M.A. also thanks the Camille and Henry Dreyfus Foundation for a Camille Dreyfus Teacher-Scholar Award (2011–2016). We thank Kan Ueji and Hiroshi Imada for assistance with the experiments, and Gordon J. Miller for useful discussions.

- 
- [1] P. J. F. Harris, Growth and structure of supported metal catalyst particles, *Int. Mater. Rev.* **40**, 97 (1995).
- [2] P. A. Thiel, M. Shen, D.-J. Liu, and J. W. Evans, Critical review: Adsorbate-enhanced transport of metals on metal surfaces: Oxygen and sulfur on coinage metals, *J. Vac. Sci. Technol. A* **28**, 1285 (2010).
- [3] G. S. Parkinson, Z. Novotny, G. Argentero, M. Schmid, J. Pavelec, R. Kosak, P. Blaha, and U. Diebold, Carbon monoxide-induced adatom sintering in a Pd-Fe<sub>3</sub>O<sub>4</sub> model catalyst, *Nat. Mater.* **12**, 724 (2013).
- [4] G. L. Kellogg, Hydrogen promotion of surface self-diffusion on Rh(100) and Rh(311), *Phys. Rev. B* **55**, 7206 (1997).
- [5] S. Horch, H. T. Lorensen, S. Helveg, E. Laegsgaard, I. Stensgaard, K. W. Jacobsen, J. K. Norskov, and F. Besenbacher, Enhancement of surface self-diffusion of platinum atoms by adsorbed hydrogen, *Nature (London)* **398**, 134 (1999).
- [6] A. R. Layson and P. A. Thiel, Testing realistic environments for metal film growth and aging: Chemical insights into the effect of oxygen on Ag/Ag(100), *Surf. Sci.* **472**, L151 (2001).
- [7] A. R. Layson, J. W. Evans, and P. A. Thiel, Additive-enhanced coarsening and smoothing of metal films: Complex mass-flow dynamics underlying nanostructure evolution, *Phys. Rev. B* **65**, 193409 (2002).
- [8] P. Maksymovych, O. Voznyy, D. B. Dougherty, D. C. Sorescu, and J. T. Yates, Jr., Gold adatom as a key structural component in self-assembled monolayers of organosulfur molecules on Au(111), *Prog. Surf. Sci.* **85**, 206 (2010).
- [9] P. J. Feibelman, Formation and diffusion of S-decorated Cu clusters on Cu(111), *Phys. Rev. Lett.* **85**, 606 (2000).

- [10] W. L. Ling, N. C. Bartelt, K. Pohl, J. de la Figuera, R. Q. Hwang, and K. F. McCarty, Enhanced self-diffusion on Cu(111) by trace amounts of S: Chemical-reaction-limited kinetics, *Phys. Rev. Lett.* **93**, 166101 (2004).
- [11] K. Morgenstern, E. Laegsgaard, and F. Besenbacher, Sintering of cobalt nanoclusters on Ag(111) by sulfur: Formation of one-, two-, and three-dimensional cobalt sulfide, *Surf. Sci.* **602**, 661 (2008).
- [12] M. Shen, D.-J. Liu, C. J. Jenks, P. A. Thiel, and J. W. Evans, Accelerated coarsening of Ag adatom islands on Ag(111) exposed to S: Mass-transport mediated by Ag-S complexes, *J. Chem. Phys.* **130**, 094701 (2009).
- [13] M. Shen, D.-J. Liu, C. J. Jenks, and P. A. Thiel, The effect of chalcogens (O, S) on coarsening of nanoislands on metal surfaces, *Surf. Sci.* **603**, 1486 (2009).
- [14] M. Shen, S. M. Russell, D.-J. Liu, and P. A. Thiel, Destabilization of Ag nanoislands on Ag(100) by adsorbed sulfur, *J. Chem. Phys.* **135**, 154701 (2011).
- [15] M. Foss, R. Feidenhans'l, M. Nielsen, E. Findeisen, R. L. Johnson, T. Buslaps, I. Stensgaard, and F. Besenbacher, Sulfur chemisorption on Ni(111): The clock structure of the  $(5\sqrt{3} \times 2)S$  phase, *Phys. Rev. B* **50**, 8950(R) (1994).
- [16] M. Foss, R. Feidenhans'l, M. Nielsen, E. Findeisen, T. Buslaps, R. L. Johnson, and F. Besenbacher, Sulfur induced Cu<sub>4</sub> tetramers on Cu(111), *Surf. Sci.* **388**, 5 (1997).
- [17] S. M. Russell, Y. Kim, D.-J. Liu, J. W. Evans, and P. A. Thiel, Structure, formation, and equilibration of ensembles of Ag-S complexes on an Ag surface, *J. Chem. Phys.* **138**, 071101 (2013).
- [18] E. Wahlström, I. Ekvall, H. Olin, S. A. Lindgren, and L. Wallden, Observation of ordered structures for S/Cu(111) at low temperature and coverage, *Phys. Rev. B* **60**, 10699 (1999).
- [19] E. Wahlström, I. Ekvall, T. Kihlgren, H. Olin, S. A. Lindgren, and L. Wallden, Low-temperature structure of S/Cu(111), *Phys. Rev. B* **64**, 155406 (2001).
- [20] G. Kresse and J. Furthmüller, Efficiency of ab-initio total energy calculations for metals and semiconductors using a plane-wave basis set, *Comput. Mater. Sci.* **6**, 15 (1996).
- [21] P. E. Blöchl, Projector augmented-wave method, *Phys. Rev. B* **50**, 17953 (1994).
- [22] J. P. Perdew, K. Burke, and M. Ernzerhof, Generalized gradient approximation made simple, *Phys. Rev. Lett.* **77**, 3865 (1996).
- [23] J. Tersoff and D. R. Hamann, Theory and application for the scanning tunneling microscope, *Phys. Rev. Lett.* **50**, 1998 (1983).
- [24] J. Tersoff and D. R. Hamann, Theory of the scanning tunneling microscope, *Phys. Rev. B* **31**, 805 (1985).
- [25] G. te Velde, F. M. Bickelhaupt, E. J. Baerends, C. Fonseca Guerra, S. J. A. van Gisbergen, J. G. Snijders, and T. Ziegler, Chemistry with ADF, *J. Comput. Chem.* **22**, 931 (2001).
- [26] E. van Lenthe, E. J. Baerends, and J. G. Snijders, Relativistic total energy using regular approximations, *J. Chem. Phys.* **101**, 9783 (1994).
- [27] E. van Lenthe, A. Ehlers, and E.-J. Baerends, Geometry optimizations in the zero order regular approximation for relativistic effects, *J. Chem. Phys.* **110**, 8943 (1999).
- [28] H. Häkkinen, The gold-sulfur interface at the nanoscale, *Nat. Chem.* **4**, 443 (2012).
- [29] P. D. Jadzinsky, G. Calero, C. J. Ackerson, D. A. Bushnell, and R. D. Kornberg, Structure of a thiol monolayer-protected gold nanoparticle at 1.1 Å resolution, *Science* **318**, 430 (2007).
- [30] D.-J. Liu, Density functional analysis of key energetics in metal homoepitaxy: Quantum size effects in periodic slab calculations, *Phys. Rev. B* **81**, 035415 (2010).